frontiers in Astronomy and Space Sciences

ORIGINAL RESEARCH
published: 29 October 2021
doi: 10.3389/fspas.2021.745264

# Quantification of Cold-Ion Beams in a Magnetic Reconnection Jet

*Yu-Xuan Li[1], Wen-Ya Li[2]*, Bin-Bin Tang[2]*, C. Norgren[3], Jian-Sen He[1], Chi Wang[2], Qiu-Gang Zong[1], S. Toledo-Redondo[4,5], M. André[6], C. Chappell[7], J. Dargent[8], S. A. Fuselier[9,10], A. Glocer[11], D. B. Graham[6], S. Haaland[12,13,14], L. Kistler[15], B. Lavraud[5,16], T. E. Moore[10], P. Tenfjord[3], S. K. Vines[17] and J. Burch[9]*

[1]Institute of Space Physics and Applied Technology, Peking University, Beijing, China, [2]State Key Laboratory of Space Weather, National Space Science Center, Chinese Academy of Sciences, Beijing, China, [3]Space Plasma Physics Group, Department of Physics and Technology, University of Bergen, Bergen, Norway, [4]Department of Electromagnetism and Electronics, University of Murcia, Murcia, Spain, [5]Institut de Recherche en Astrophysique et Planétologie, Université de Toulouse, CNRS, UPS, CNES, Toulouse, France, [6]Swedish Institute of Space Physics, Uppsala, Sweden, [7]Physics and Astronomy Department, Vanderbilt University, Nashville, TN, United States, [8]Physics Department E. Fermi, University of Pisa, Pisa, Italy, [9]Southwest Research Institute, San Antonio, TX, United States, [10]Department of Physics and Astronomy, University of Texas at San Antonio, San Antonio, TX, United States, [11]NASA Goddard Space Flight Center, Greenbelt, MD, United States, [12]Max-Planck Institute for Solar Systems Research, Göttingen, Germany, [13]Birkeland Center for Space Science, University of Bergen, Bergen, Norway, [14]The University Centre in Svalbard, Longyearbyen, Svalbard, [15]Institute for the Study of Earth Oceans and Space, University of New Hampshire, Durham, NH, United States, [16]Laboratoire d'Astrophysique de Bordeaux, Univ. Bordeaux, Pessac, France, [17]Applied Physics Laboratory, Johns Hopkins University, Laurel, MD, United States

OPEN ACCESS

**Edited by:**
Olga V. Khabarova,
Institute of Terrestrial Magnetism Ionosphere and Radio Wave Propagation (RAS), Russia

**Reviewed by:**
Elena E. Grigorenko,
Space Research Institute (RAS), Russia
Tieyan Wang,
Rutherford Appleton Laboratory, United Kingdom

***Correspondence:**
Wen-Ya Li
wyli@spaceweather.ac.cn
Bin-Bin Tang
bbtang@spaceweather.ac.cn

**Specialty section:**
This article was submitted to Space Physics, a section of the journal Frontiers in Astronomy and Space Sciences

**Received:** 21 July 2021
**Accepted:** 11 October 2021
**Published:** 29 October 2021

**Citation:**
Li Y-X, Li W-Y, Tang B-B, Norgren C, He J-S, Wang C, Zong Q-G, Toledo-Redondo S, André M, Chappell C, Dargent J, Fuselier SA, Glocer A, Graham DB, Haaland S, Kistler L, Lavraud B, Moore TE, Tenfjord P, Vines SK and Burch J (2021) Quantification of Cold-Ion Beams in a Magnetic Reconnection Jet. Front. Astron. Space Sci. 8:745264. doi: 10.3389/fspas.2021.745264

Cold (few eV) ions of ionospheric origin are widely observed in the lobe region of Earth's magnetotail and can enter the ion jet region after magnetic reconnection is triggered in the magnetotail. Here, we investigate a magnetotail crossing with cold ions in one tailward and two earthward ion jets observed by the Magnetospheric Multiscale (MMS) constellation of spacecraft. Cold ions co-existing with hot plasma-sheet ions form types of ion velocity distribution functions (VDFs) in the three jets. In one earthward jet, MMS observe cold-ion beams with large velocities parallel to the magnetic fields, and we perform quantitative analysis on the ion VDFs in this jet. The cold ions, together with the hot ions, are reconnection outflow ions and are a minor population in terms of number density inside this jet. The average bulk speed of the cold-ion beams is approximately 38% larger than that of the hot plasma-sheet ions. The cold-ion beams inside the explored jet are about one order of magnitude colder than the hot plasma-sheet ions. These cold-ion beams could be accelerated by the Hall electric field in the cold ion diffusion region and the shrinking magnetic field lines through the Fermi effect.

**Keywords: cold ions, plasma moments, acceleration, magnetic reconnection, Earth's magnetotail**

## 1 INTRODUCTION

Cold (few eV) ions of ionospheric origin are widely present in the Earth's magnetosphere (Chappell et al., 1980; Moore et al., 1997; Cully et al., 2003). In the lobes of the magnetosphere, spacecraft can be positively charged to several tens of volts due to photoelectron emissions. The positive potential prevents cold ions from reaching onboard ion instrument. With large-scale convective motion, for example, magnetopause fluctuation or plasma-sheet flapping, cold ions can be accelerated via the **E**×**B** drift to overcome the positive spacecraft potential (Sauvaud et al., 2004), and be detected by an ion instrument. Besides direct measurement with particle instruments, cold ions can also be inferred

by a technique based on the wake signal of a charged spacecraft in a supersonic ion flow (Engwall et al., 2009; Li et al., 2013; André et al., 2015). Observational statistics show that cold ions dominate the plasma density in large regions of the nightside magnetosphere (e.g., lobe region) and polar regions (André and Cully, 2012). At times, the cold ions can also dominate in the dayside magnetosphere. Cold ions can play an important role in the solar wind-magnetosphere-ionosphere coupling system, including the terrestrial plasma escape and circulation and the magnetotail dynamics (Welling et al., 2015; Kistler and Mouikis, 2016; Yamauchi, 2019).

Magnetic reconnection is a fundamental and universal process to convert energy stored in the magnetic field into kinetic and thermal energies of charged particles (Priest and Forbes, 2007; Yamada et al., 2010). Magnetic reconnection is the major transport mechanism of mass, energy, and magnetic flux in the solar wind-magnetosphere coupling system, and is the predominant cause of the geomagnetic activity. In the past decade, the effects of cold ions on magnetic reconnection at the dayside magnetopause and in the magnetotail have been extensively analyzed via using *in-situ* measurements from multiple spacecraft missions (Wang et al., 2014; Toledo-Redondo et al., 2015; André et al., 2016; Li et al., 2017; Toledo-Redondo et al., 2021) and types of numerical simulation models (Aunai et al., 2011; Divin et al., 2016; Tenfjord et al., 2019; Dargent et al., 2019, 2020). At the dayside magnetopause, magnetic reconnection is typically asymmetric due to the large differences in plasma and magnetic field conditions between the magnetosheath and the magnetosphere. The gyroradii and the inertial lengths of the magnetosheath plasmas usually determine the two kinetic scales of the diffusion region, namely, ion and electron diffusion regions (Yamada et al., 2010). With the presence of cold-ion inflow from the magnetospheric side, cold ions bring a new diffusion region between the usual ion and electron diffusion regions (Toledo-Redondo et al., 2016a; Divin et al., 2016), and can push the reconnection jet towards the magnetosheath side (Cassak and Shay, 2007; Walsh et al., 2014). Li et al. (2017) present the first observation of the cold-ion outflows throughout the entire reconnection region via investigating the three-dimensional (3D) ion velocity distribution functions (VDFs). Cold-ion jets with high parallel velocities are formed on the magnetosheath side of the reconnection exhaust, and those cold ions remain relatively cold compared with the magnetosheath ions. Li et al. (2017) suggest that those fast cold-ion jets originate from the cold-ion inflow close to the X line, while the acceleration mechanism lacks detailed analysis.

In the magnetotail, the magnetic fields are oppositely directed on each side of the plasma sheet, and the plasma-sheet plasmas are hot with ion temperature of several to tens of keV. Magnetic reconnection is symmetric with homogeneous hot ion inflows from both sides. The plasma sheet boundary layer (PSBL) and lobe region always contain a certain amount of cold ions of ionospheric origin, which can affect the reconnection process in the magnetotail. One prominent feature is that cold ions create highly structured ion VDFs far from the Maxwellian shape. Among these distributions, counter-streaming cold-ion beams along the direction normal to the current sheet are frequently observed in the ion diffusion region both in observations and simulations (Fujimoto et al., 1996; Hoshino et al., 1998; Nagai et al., 1998; Shay et al., 1998; Wygant et al., 2005; Divin et al., 2016; Dai et al., 2021). The counter-streaming cold-ion beams are suggested to be accelerated by the Hall electric field along the normal direction at the separatrix, which is mostly along **Z** direction of Geocentric Solar Ecliptic (GSE) coordinates. The electric potential well across the separatrix is $B_X^2/2q_eN_0\mu_0$, where $B_X$ and $N_0$ are the reconnection magnetic field and plasma number density in the inflow, $q_e$ is the unit of charge and $\mu_0$ is the magnetic permeability of free space (Wygant et al., 2005; Divin et al., 2016; Zaitsev et al., 2021). This electric potential can accelerate cold ions to the inflow Alfvén speed $V_A = B_X/\sqrt{\mu_0 m_i N_0}$, when the width of the separatrix is comparable to the cold-ion gyroradius. Using a hybrid simulation model, Aunai et al. (2011) show that the angular aperture of the potential well and the bouncing motion between the separatries make the cold ions transfer the kinetic energy gained from the $V_Z$ component to $V_X$.

Besides the acceleration by the Hall electric field in the ion diffusion region, the Fermi mechanism (slingshot effect) and the reconnection electric field can also be important for cold-ion acceleration in the reconnection exhaust. Several studies report counter-streaming cold-ion beams observed in bursty bulk flows (BBFs) and analyze acceleration mechanisms and ion anisotropic instabilities associated with these beams (Eastwood et al., 2015; Hietala et al., 2015; Birn et al., 2017; Runov et al., 2017; Xu et al., 2019). BBFs are widely interpreted as magnetic reconnection jets (Angelopoulos et al., 1992; Nagai et al., 1998; Birn et al., 2011) and can transport significant amount of magnetic fluxes and plasmas towards Earth (Baumjohann et al., 1990; Angelopoulos et al., 1992, 1994). Eastwood et al. (2015) find that counter-streaming beams are sourced from the thermal population in the preexisting plasma sheet and are accelerated by the reconnection electric field. Birn et al. (2017) show that the beam ions are from the low-energy lobe regions. These beams are firstly accelerated by the **E**×**B** drift motion and then by the slingshot effect of the earthward convecting BBF. A similar process is also described by Xu et al. (2019). In the previous studies, the counter-streaming cold-ion beams are mostly observed near the front edge of the reconnection jet, and quantitative studies analyzing the acceleration are primarily via numerical simulations. The existence and dynamics of the cold ions in an entire reconnection jet still lack quantitative analysis using *in-situ* observations. In this study, we perform a more comprehensive survey of ion VDFs in a magnetotail crossing by the Magnetospheric Multiscale (MMS) spacecraft. Various types of ion VDFs with cold-ion beams are observed inside a magnetic reconnection jet, and plasma partial moments of the cold ions are computed to investigate their dynamics through the reconnection process.

## 2 OBSERVATIONS

In-situ observations from NASA's MMS mission (Burch et al., 2016) are utilized for this study. MMS was launched on March 13,

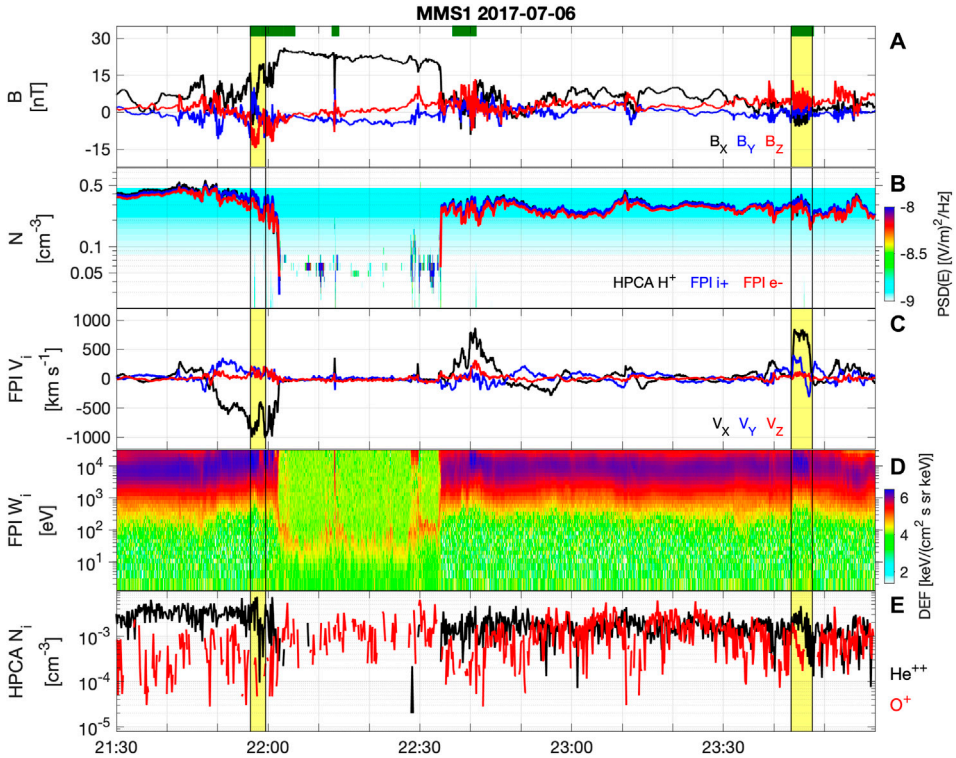


**FIGURE 1 |** MMS observation of the Earth's magnetotail on July 06, 2017. MMS1 data of **(A)** magnetic field **B**, **(B)** number densities of hydrogen ($H^+$, black) from HPCA, all ions (blue) and electrons (red) from FPI and electron number density derived from the Langmuir waves observed by EDP, **(C)** ion bulk velocity $\mathbf{V}_i$ from FPI, **(D)** FPI ion omnidirectional differential energy flux, **(E)** number densities of $He^{++}$ (black) and $O^+$ (red) ions from HPCA. All vectors are presented in GSE coordinates, which are close to Geocentric Solar Magnetospheric (GSM) coordinates in this event. The horizontal green bars in the top of **(A)** denote the burst-mode time intervals, and detailed analysis of the ion VDFs in the two yellow-shaded intervals are presented in the following figures.

2015 and consists of four identical spacecraft designed to study the kinetic-scale physics of magnetic reconnection in the Earth's magnetosphere. In this study, we use magnetic field data from the FluxGate Magnetometer (FGM) (Russell et al., 2016) and electric field data from the Electric Double Probe (EDP) (Ergun et al., 2016; Lindqvist et al., 2016). The ion data are from the Fast Plasma Investigation (FPI) (Pollock et al., 2016) sampled at 4.5 s for the fast mode and 0.15 s for the burst mode, and also, from the mass-resolved instrument Hot Plasma Composition Analyzer (HPCA) (Young et al., 2016) at 10 s resolution.

We investigate an MMS magnetotail crossing from 21:30:00 to 24:00:00 UT on July 06, 2017. The four spacecraft moved from [−24.6, −0.8, 5.2] $R_E$ (Earth radii) to [−24.5, −1.4, 5.4] $R_E$ (GSE) during this time interval. Owing to a small spacecraft separation ( ~15 km), observations from the four spacecraft are nearly identical, and thus, we show results primarily from MMS1. An overview of the MMS1 observations is presented in **Figure 1**, and the data are in fast mode. The panels from top to bottom show 1) magnetic field **B**, 2) number densities of ions and electrons, 3) ion bulk velocities from FPI, 4) FPI ion omnidirectional differential energy flux, and 5) number densities of $He^{++}$ and $O^+$ ions from HPCA. In **Figure 1B**, the number densities of $H^+$ from HPCA, all ions from FPI and electrons from FPI are shown in black, blue and red, respectively. The three curves almost overlap with each other, indicating reliable number density results. The MMS fleet is initially located in the plasma sheet, characterized by weak magnetic field (**Figure 1A**) and high-density ( ~0.5 $cm^{-3}$) and hot ( ~4,500 eV) ions. From 21:49:00 to 22:02:00 UT, MMS1 observes a strong tailward ion flow, with a peak $V_X$ reaching -1,000 km $s^{-1}$. Such a strong ion flow indicates ongoing reconnection and that the spacecraft are located tailward of the reconnection X line. In this tailward ion jet, the $B_X$ component is mostly positive, indicating that MMS cross the northern part of the ion jet.

At 22:02:00 UT, we identify a separatrix of the reconnection exhaust, where B increases, plasma number density decreases, ion bulk velocity decreases, and energetic particles vanish (see **Supplementary Figure S1** in **Supplementary Material** for more details). Then, MMS1 enters the lobe region until 22:34:00 UT. As shown by the ion energy flux in **Figure 1D**, cold ions of ionospheric origin, with ~10 eV thermal energy, are present in the lobe region, while their total energy can reach 100 eV due to the **E×B** drift motion. In the lobe, the penetrating radiation leads to a nearly constant background from the lowest to the highest energy channels in the FPI ion measurement unit (Gershman et al., 2019), as seen by the green fluxes in **Figure 1D**. Thus, the FPI ion number density from the integral over the whole energy range is overestimated. Besides, the FPI electron measurement unit cannot provide reliable electron moment data in the lobe because of the low thermal energy and the photoelectron contamination (Gershman et al., 2019). So, we take the

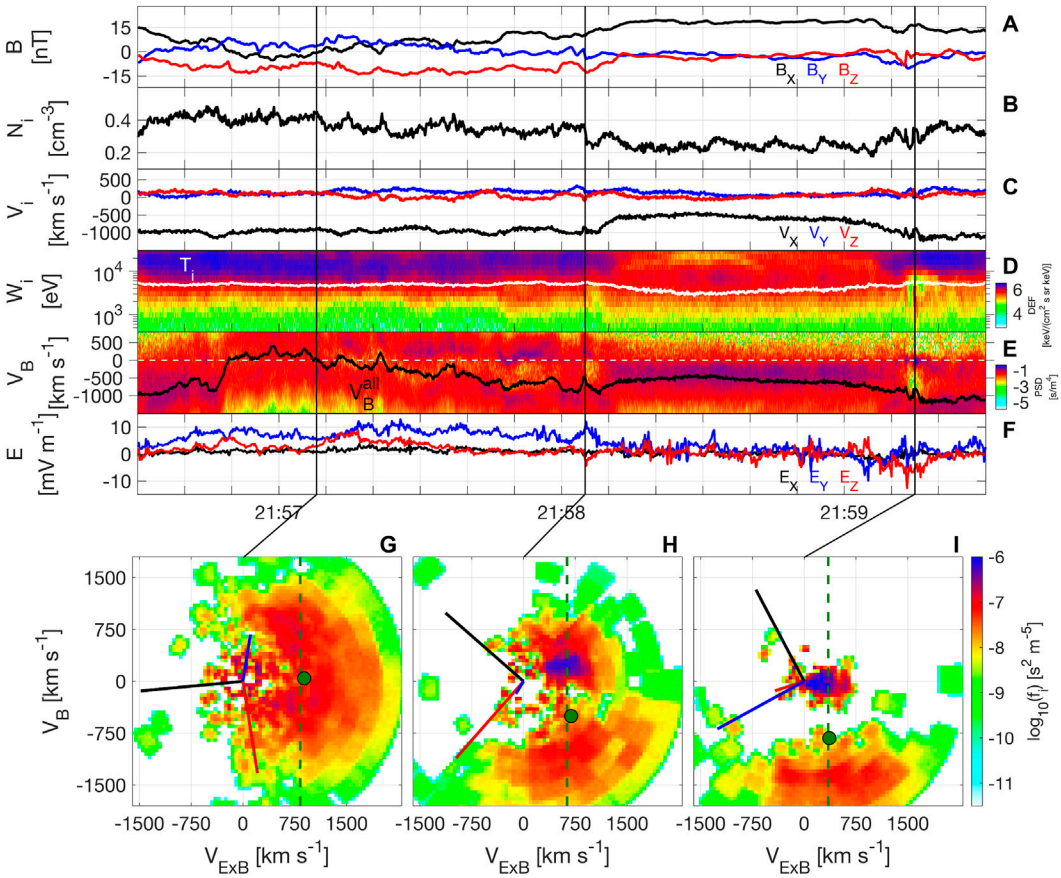


**FIGURE 2 |** Cold ions inside the tailward ion jet. **(A) B**. **(B)** $N_i$. **(C)** $\mathbf{V}_i$. **(D)** FPI ion omnidirectional differential energy flux with ion temperature (white curve). **(E)** Reduced ion VDF integrated over the directions perpendicular to the magnetic field. The black solid curve shows the parallel ion bulk speed $V_B^{all}$ of all ions, and the white dashed line denotes $V_B = 0$. **(F)** Electric field **E**. **(G)–(I)** Two-dimensional (2D) reduced ion VDFs in the $\mathbf{V}_{ExB}$-$\mathbf{V}_B$ plane at times indicated by the three vertical lines in **(A)–(F)**. In **(G)–(I)**, the green dots represent the ion bulk velocities, and the vertical green dashed lines show the electric-field drift speeds ($|\mathbf{E}\times\mathbf{B}/B^2|$). The GSE-X (black), Y (blue) and Z (red) directions normalized by 1,500 km s$^{-1}$ are projected in **(G)–(I)**.

number density (0.03–0.05 cm$^{-3}$) estimated from the waves at the electron plasma frequencies, as illustrated by the color-coded spectrum in **Figure 1B**. In the lobe, oxygen ions measured by HPCA have number densities about 0.0005–0.002 cm$^{-3}$ (**Figure 1E**), and hydrogen is thus the primary ion species in terms of number density. From 22:13:04 to 22:13:15 UT, MMS cross a separatrix of the reconnection exhaust back and forth quickly (see **Supplementary Figure S2** in **Supplementary Material** for details). Based on the observations during this time interval, Alm et al. (2018) analyzed the role of cold ions in the separatrix layer. They find that the cold ions account for ~ 30% of the total ion number density and can significantly influence the Hall physics of reconnection. After 22:34:00 UT, MMS1 crosses back to the plasma sheet and sees two strong earthward ion jets, with a$V_X$ peak reaching 860 km s$^{-1}$. $O^+$ ions, as tracers of cold ionospheric ions, are continuously observed inside the plasma sheet shown in **Figure 1**, and have similar number densities with those in the lobe. Meanwhile, $He^{++}$ ions can be used as tracers of solar wind ions, and are also continuously observed in the plasma sheet. Thus, both the ionospheric and solar-wind ions are the ion sources of the plasma sheet in our event, even through the two sources are indistinguishable from the FPI ion energy flux panel (**Figure 1D**). We explore the 3D ion VDFs in the tailward and earthward reconnection jets and characterize different types of ion VDFs with cold-ion beams. In the following, we present results from the two time intervals indicated by the yellow-shaded bars in **Figure 1**.

**Figures 2A–F** present an overview of the tailward ion jet in the time interval indicated by the left yellow-shaded bar in **Figure 1**. Here, burst-mode data are used. In this jet, $V_X$ varies between −1,240 km s$^{-1}$ and −430 km s$^{-1}$, and ions with distinct energy fluxes are all above 500 eV in the spacecraft frame (**Figure 2D**). **Figure 2E** shows the phase space density of the reduced ion VDF projected on to the magnetic field directions, and the black curve represents the parallel bulk velocity $\mathbf{V}_B^{all}$ of all ions. One can clearly see complicated structures in this reduced ion VDF panel. To categorize the ions in this tailward jet, we perform a systematic survey of all the ion VDFs in the time interval of **Figure 2** and find three types of ion VDFs inside. **Figures 2G–I** show 2D reduced ion VDF examples in the $\mathbf{V}_{E\times B}$-$\mathbf{V}_B$ plane, as they clearly show the overall structures in the distribution functions. At times like 21:57:08 UT, $\mathbf{V}_B^{all}$ is close to the ion VDF peaks, denoting that there exists only a single energetic ion

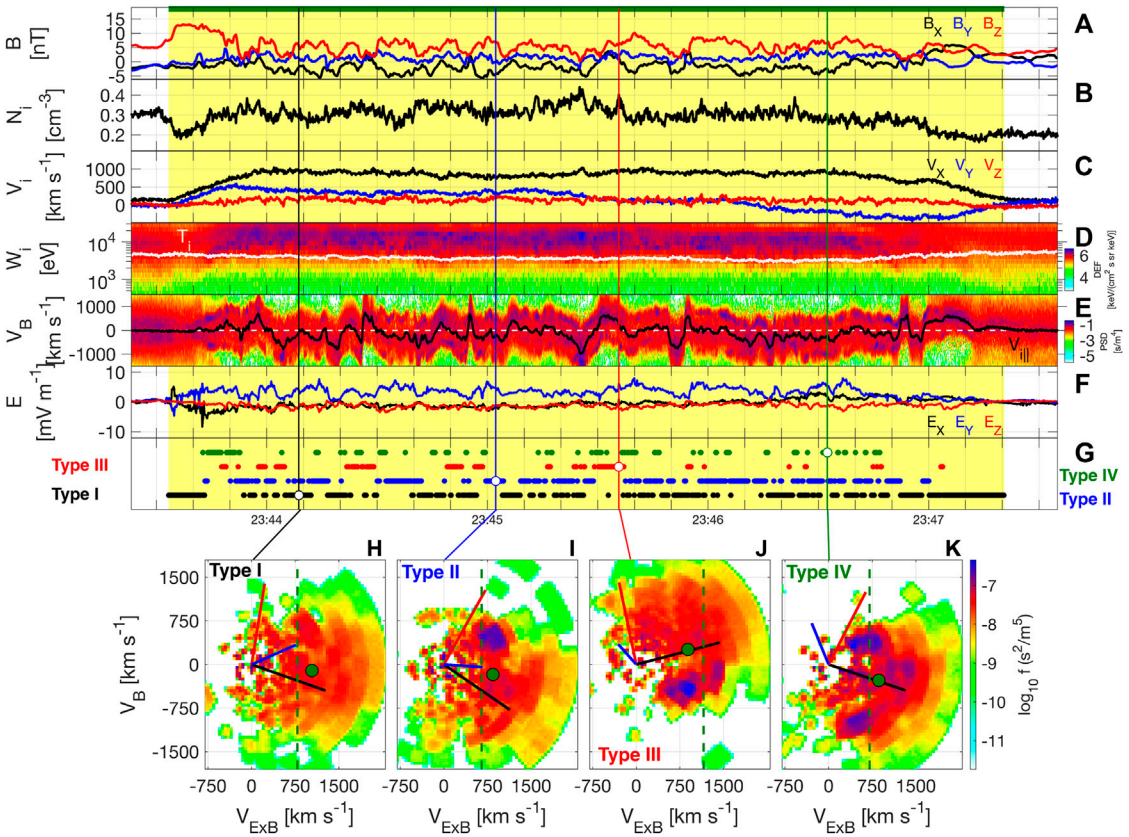


**FIGURE 3 |** Four types of ion velocity distribution functions (VDFs) in the earthward ion jet. **(A) B**. The green horizontal bar denotes the ion jet interval. **(B)** $N_i$. **(C)** $\mathbf{V}_i$. **(D)** FPI ion omnidirectional differential energy flux with ion temperature (white curve). **(E)** Reduced ion VDF integrated over the directions perpendicular to the magnetic field. The black solid curve shows the parallel ion bulk speed $V_{i\|}$, and the white dashed line denotes $V_{i\|} = 0$. **(F)** Electric field **E**. **(G)** Ion VDF types inside the ion jet. **(H)–(K)** Examples of the four-type ion VDFs at times indicated by the four vertical lines in **(A)–(G)**. **(H)–(K)** are in the same format with **Figures 2G–I**.

population of plasma-sheet origin (see **Figure 2G**). The hot population in **Figure 2G** has a temperature of 4.6 keV and follows **E×B** drift motion (green vertical dashed line), with negligible $\mathbf{V}_B$. In GSE coordinates, it moves predominantly along -**X** direction. From 21:59:12 to 21:59:19 UT, MMS1 observes two distinct ion populations in the FPI ion energy flux plot (**Figure 2D**). One energetic population has energy above 8 keV and originates from the plasma sheet. The other population has energies below 5 keV. An example of the ion VDFs within this interval is presented in **Figure 2I**. At this time, the magnetic field is mostly along the +**X** direction (**Figure 2A**), and its magnitude is close to that in the lobe (see **Figure 1**). The electric field is dominated by the -**Z** component, indicating Hall electric field in the northern separatrix layer of the magnetotail reconnection in the magnetotail (Wygant et al., 2005; Eastwood et al., 2007). The two ion populations have the same **E×B** drift velocity. The hot population has a large negative $\mathbf{V}_B$, and its bulk velocity is predominantly along the -**X** direction in GSE coordinates. The cold population has negligible $\mathbf{V}_B$ and moves along the -**Y** direction. Those cold ions can modify the balance of the Hall electric field at the separatrix, which has been extensively analyzed by previous studies using *in-situ* data (Toledo-Redondo et al., 2015; André et al., 2016; Alm et al., 2018) and numerical simulation models (Dargent et al., 2017; Toledo-Redondo et al., 2018).

From 21:57:12 UT to 21:58:10 UT, MMS1 also observes two distinct populations in the reduced ion VDFs shown in **Figure 2E**, even though the two populations are not distinguishable from the FPI ion energy flux (**Figure 2D**). **Figure 2H** displays an example of the ion VDFs in this time interval. The properties of the hot population are similar to those shown in **Figure 2I**. The cold population follows **E×B** drift ( ~630 km s$^{-1}$) motion and has a small ( ~200 km s$^{-1}$) positive $\mathbf{V}_B$. Its bulk velocity is predominantly along the -**Z** direction in GSE. These cold-ion beams may originate from the northern lobe. A small bulk speed ( ~660 km s$^{-1}$) of this cold population suggests that those beams may be not from the cold-ion inflow close to the X line. They may experience an acceleration process as discussed previously by Birn et al. (2017). The cold ions are probably accelerated by the **E×B** drift motion when crossing a distant separatrix, and are further accelerated by the Fermi mechanism as the cold ions convect together with the shrinking magnetic field lines. Another prominent feature between the cold populations shown in **Figures 2H,I** is that the cold population in **Figure 2H** is clearly thermalized, and we discuss that in the following section. In the earthward ion jet between 22:36:00 UT and 22:47:00 UT,

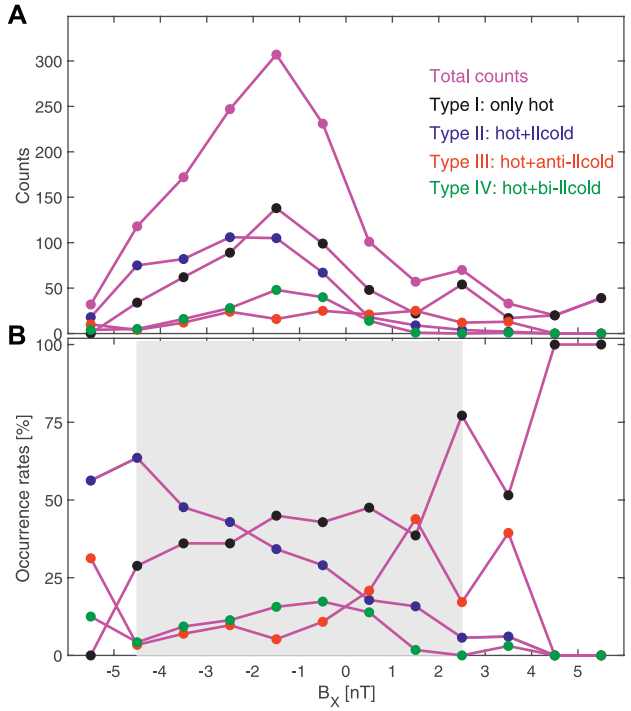


**FIGURE 4 |** Statistics of the four types of ion VDFs along $B_X$. **(A)** Counts profiles along $B_X$. The magenta curve shows the total counts, and the rest of the curves show the four types of VDFs. **(B)** Occurrence rates. The gray shadow highlights the interval with total counts over 50.

MMS observe similar features of the ion VDFs as those presented in **Figure 2**.

MMS see much more complicated features of cold-ion beams in the earthward ion jet between 23:43:23 UT and 23:47:53 UT (denoted by the right yellow-shaded bar in **Figure 1**). **Figures 3A–F** display a detailed overview of this ion jet using burst-mode data. MMS are originally located in the stagnant plasma sheet. When a dipolarization front (Nakamura et al., 2002; Runov et al., 2009; Fu et al., 2013) arrives at MMS at ~23:43:34 UT, the plasma density drops from 0.31 $cm^{-3}$ to 0.20 $cm^{-3}$ and the magnetic field $B_Z$ component increases from 5 to 13 nT. The earthward flow speed subsequently increases to its maximum values, with $aV_X$ peak reaching 1,040 km $s^{-1}$. This kind of fast ion flow is frequently interpreted as an earthward bursty bulk flow (BBF) driven by magnetic reconnection with an X line located tailward of the spacecraft. In **Figure 3**, we use a yellow-shaded bar to highlight the BBF or the jet interval. The average $N_i$ of the jet is approximately 0.29 $cm^{-3}$, which is similar to that of the nearby plasma sheet. The average $T_i$ is 3.8 keV, with a small temperature anisotropy ($T_{i\|}/T_{i\perp}$ ~0.92). After a detailed survey of all the ion VDFs, we find four types of ion VDFs inside the jet shown in **Figure 3**: Type I consists of only a single hot plasma-sheet population (see an example shown by **Figure 3H**), Type II consists of a hot population and a cold population with a positive $\mathbf{V}_B$ (see **Figure 3I**), Type III consists of a hot population and a cold population with a negative $\mathbf{V}_B$ (see **Figure 3J**), and Type IV consists of a hot population with counter-streaming cold populations (see **Figure 3K**). We categorize all the ion VDFs of this earthward ion jet, and the results are presented by colored dots in **Figure 3G**. In **Figures 3H–K**, the green dots denote the projected ion bulk velocities in the $V_{E\times B}$-$V_B$ plane, and the green vertical dashed lines represent the **E**×**B** drift speeds. The small discrepancy between the two speeds is likely from the errors (0.5–1.0 mV $m^{-1}$) in electric field (Lindqvist et al., 2016) or could be caused by weak demagnetization of the ions. In GSE coordinates, all ions propagate earthward (illustrated by the black lines in **Figures 3H–K**). The large positive and negative $V_B$ components of the cold ions correspond to the large positive and negative $V_Z$ components (**Figures 3I–K**), respectively.

Previous studies like Eastwood et al. (2015) and Xu et al. (2019) explored the kinetic behavior of counter-streaming cold ions at the leading edges of the reconnection jets, with particular focus on the vicinity of dipolarization front. The cold-ion beams investigated in their works may originate from ions in the preexisting plasma sheet or the ionosphere and are swept up directly by a dipolarization front. In our study, we do not find the existence of isolated cold-ion beams in the region close to the dipolarization front, which could be due to the phase-space mixing by cold-ion thermalization. We find four types of ion VDFs widely distributed over the entire observed part of the jet. The cold-ion beams have total energies all above ~3 keV and mix together with the plasma-sheet hot ions in the spectrogram of the differential energy flux (**Figure 3D**), and one can only distinguish cold ions in three-dimensional VDFs. This is different from the cold ions reported in Eastwood et al. (2015) and Xu et al. (2019), where the total energies of cold ions are lower than those of hot ions and one can easily see them in the spectrograms of the differential energy fluxes.

In the magnetotail, the $B_X$ component can be used as a guide to determine the normal distance to the plasma-sheet neutral line ($B_X$ = 0). **Figure 4A** shows the count profiles of the four types of ion VDFs along $B_X$. MMS spend most of the time in the southern exhaust, and most of the counts are therefore in the negative $B_X$ region, where Type I and Type II VDFs clearly dominate. **Figure 4B** presents the occurrence rates of the four-type ion VDFs, and the gray shadow highlights the results with total counts over 50. Despite the large variation due to relatively low counts, one can conclude that the occurrence rate of Type I is nearly constant. The occurrence rate of Type II decreases gradually along $B_X$ or from the southern to the northern sides of the neutral line. Conversely, the occurrence rate of Type III increases gradually along $B_X$. The occurrence rate of Type IV peaks at the neutral line. Therefore, the antiparallel beams are predominantly observed in the northern side of the neutral sheet, and the parallel beams are predominantly observed on the southern side. The majority of cold-ion beams were found to be approaching the neutral sheet, with a smaller subset of VDFs also showing cold ion populations moving away from the neutral sheet. This indicates that there is some mechanism that either prevents cold ions from crossing far into the opposite exhaust, that the cold-ion populations are no longer cold after the neutral sheet crossing (heating), or that they can not be distinguished from the hotter background.

The distribution of VDFs shown in **Figure 4B** may be generated by several processes. First, MMS observe the

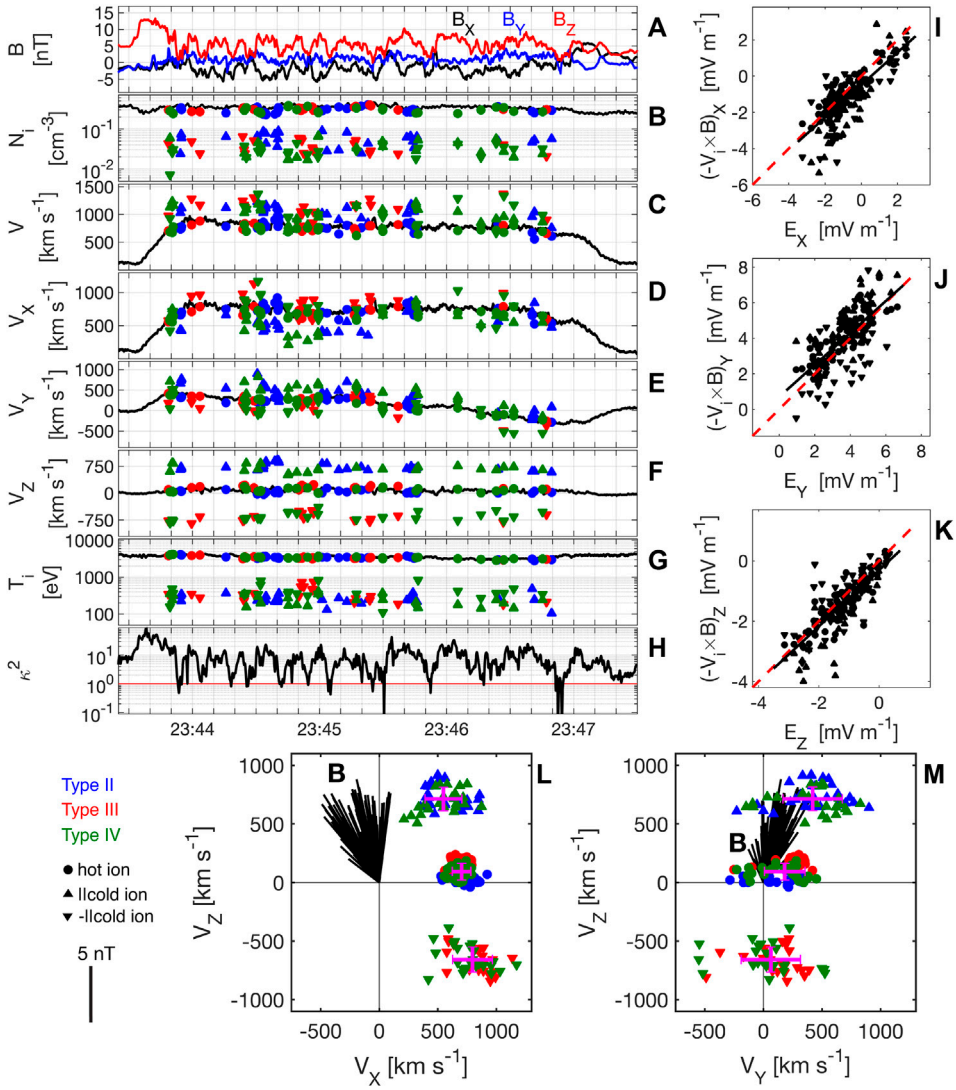


**FIGURE 5 |** Partial moments of the cold-ion beams and the hot ions inside the earthward ion jet. Those ions are from the three types (Types II, III and IV) with cold ions. Types II, III and IV are colored in blue, red and green, respectively. The partial-moment results of the hot, parallel cold and anti-parallel cold ions are marked by circles, upward-pointing triangles and downward-pointing triangles, respectively. **(A) B**. **(B)** $N_i$ of all ions (black curve) and cold and hot ions from partial moments. **(C)** Ion bulk speed V. **(D)–(F)** Three components of the ion bulk velocities $V_i$. The black curves are the average bulk velocities. **(G)** $T_i$. **(H)** Adiabatic parameter defined by $\kappa^2 = \frac{R_B}{\rho_{ci}}$ (Büchner and Zelenyi, 1989), where $R_B$ is magnetic field curvature radius and $\rho_{ci}$ is the gyroradius of the 320 eV cold ions. **(I)–(K)** Scatter plots of the measured **E** from EDP and the convection electric field **(-V$_i$×B)** of hot and cold ions from selected data points. The black dashed lines denote slope = 1, and the red dashed lines are the linear fits of the partial-moment results. **(L)–(M)** Scatter plots of the ion bulk velocity of the selected points. The crosses present the averages and the standard deviations, and the black lines show the normalized magnetic fields.

northern (see **Figure 1**) and southern lobes on July 6,2,017 and see cold ions in both lobes. As an example shown in **Figure 1D**, the energy fluxes of the cold ions in the lobe are intermittent, indicating that the cold ions inflowing into the reconnection region could be patchy. Secondly, when cold ions enter the separatrices close to the X line (e.g., the cold-ion diffusion region), numerical simulations (Aunai et al., 2011; Divin et al., 2016) show that the cold ions bounce within an electrostatic potential well between the separatrices. The distribution feature in **Figure 4B** could be a statistical result of the bouncing motions of the cold ions inflowing from both lobes. Finally, as shown in **Figure 3A**, MMS see large-amplitude fluctuations in magnetic field, which may be convected from the upstream exhaust region or be driven by the ion temperature anisotropy associated with cold-ion beams (Hietala et al., 2015). Besides, the minimum curvature radii of the magnetic field lines in this event are comparable to the gyroradii of the cold ions (as shown by **Figure 5H**). Plasma waves and the curved magnetic field lines with small curvature radii can scatter and thermalize the cold ions when moving from one side of the neutral line to the other side, and thus, can mix them with the plasma-sheet hot ions. The distributions in **Figure 4B** could be combinational results of those three effects.

**TABLE 1 |** Average partial moments of the hot and cold ions of the selected data points shown in **Figure 5**

| | Hot ion | Parallel cold ion | Anti-parallel cold ion |
|---|---|---|---|
| $N_i$ [$cm^{-3}$] | 0.30 ± 0.04 | 0.05 ± 0.02 | 0.03 ± 0.01 |
| $T_i$ [eV] | 3,430 ± 290 | 250 ± 80 | 390 ± 180 |
| $V_i$ [km $s^{-1}$] | 757 ± 71 | 1,034 ± 124 | 1,069 ± 175 |
| $V_{E\times B}$ [km $s^{-1}$] | 664 ± 118 | 688 ± 118 | 645 ± 135 |
| $V_X$ [km $s^{-1}$] | 704 ± 79 | 548 ± 157 | 796 ± 170 |
| $V_Y$ [km $s^{-1}$] | 182 ± 173 | 420 ± 254 | 63 ± 253 |
| $V_Z$ [km $s^{-1}$] | 93 ± 72 | 713 ± 100 | -657 ± 108 |

## 3 QUANTIFICATION OF COLD-ION BEAMS IN THE EARTHWARD JET

In order to study the dynamics of the cold-ion beams inside the jet, we utilize the same technique as used in Li et al. (2017) (see supporting information of that paper and **Supplementary Figure S3** in **Supplementary Material** for more details) to compute partial moments of the hot and cold populations. First, we select data points of the three types of ion VDFs with cold ions with most coverage of the variant magnetic field conditions. Then, we separate the cold and hot populations for each ion VDF in three-dimensional velocity space and compute their partial moments, including number density, bulk velocity and ion temperature. The results are presented in **Figure 5**, and the average results with standard deviations are listed in **Table 1**. In **Figures 5B–G, L,M**, the partial-moment results of the three-type VDFs (Types II, III and IV) with cold ions are labeled in blue, red and green, respectively. The hot ions from all three types are marked by circles. The parallel cold-ion beams from Types II and IV VDFs are marked by the upward-pointing triangles, while the anti-parallel beams from Types III and IV are marked by the downward-pointing triangles. The black lines in **Figures 5L,M** denote the magnetic fields of the selected data points for the partial-moment calculations. **Figures 5I–K** show the comparison between the measured electric field from EDP and the convection electric field ($-\mathbf{V}_i\times\mathbf{B}$) of the hot and cold ions from our partial-moment calculations. A good consistency of the three components means that the ions in the investigated jet are mainly frozen-in with the magnetic field lines. Also, it demonstrates a relatively good reliability of our partial-moment calculation via separating multiple populations from one VDF.

As presented in **Table 1**, the average number density ( ~0.04 $cm^{-3}$) of the cold-ion beams is comparable to that of the cold ions in the lobe and approximately 13% of that of the hot ions inside the jet. Even though the cold ions have large peak VDFs in velocity space, they are still minor populations in this investigated event. As shown by the circles in **Figure 5C**, the bulk velocities of the hot ions from the partial-moment calculations are close to the average bulk velocities (black curve) of all ions. This is consistent with the partial-moment number density results. All of the hot ions convect earthward, and their speed $V_i^H$ ( ~760 km $s^{-1}$) is close to the **E×B** drift speed. As shown in **Figures 5C–F**; **Table 1**, all the cold-ion beams move earthward, meaning that all those ions are outflow ions of reconnection. The parallel cold ions have large positive $V_Z$ component ( ~710 km $s^{-1}$), and the anti-parallel ones have large negative $V_Z$ component ( ~-660 km $s^{-1}$). The bulk speed ( ~1,050 km $s^{-1}$) of the cold-ion beams is approximately 38% larger than that of the hot ions, which is predominantly contributed by the $V_Z$ or parallel component.

It is difficult to know the acceleration process from the observational aspect. Here, we find a similarity between the velocity patterns in **Figures 5L,M** and previous numerical results (Aunai et al., 2011; Divin et al., 2016) and suggest that the cold ions inside this investigated jet may come from the region close to the X line. Cold ions are demagnetized while crossing the separatrices close to the X line (Toledo-Redondo et al., 2016a; Divin et al., 2016), and are accelerated primarily by the Hall electric field, while the beams can remain relatively cold. The cold-ion beams may bounce for several times within the Hall electrostatic potential well, and get significant $V_Z$ and $V_X$ components. Then, the accelerated cold-ion beams could be further accelerated by the shrinking magnetic field lines due to the Fermi effect. One can find a characteristic example of such acceleration process from **Figure 5** of Divin et al. (2016). This process could be responsible for the 38% extra speed at the MMS observation location.

Using Cluster data, Toledo-Redondo et al. (2016b) showed that cold ions can be heated by the large electric field gradient when crossing a separatrix boundary. Graham et al. (2017) analyzed a magnetopause reconnection event with cold ions and found lower-hybrid waves at the separatrix driven by the ion-ion streaming instability between the cold ions and the magnetosheath ions. The lower-hybrid waves can contribute to the cold-ion heating. Norgren et al. (2021) showed that the cold ions can be heated through a combination of thermalization at the separatrices and pitch angle scattering in the curved magnetic field around the neutral plane. Here, we calculate the temperature ( ~320 eV) of the cold-ion beams inside the reconnection jet, which corresponds to about 6% of the total energy in the spacecraft frame. The cold-ion beams are approximately one order of magnitude colder than the hot ions, while the cold-ion beams are thermalized compared to the cold ions ( ~10 eV) in the lobe. The large electric-field gradient at the separatrix and the scattering effect by the kinetic waves (see **Supplementary Figure S4** in **Supplementary Material** for more details) and small magnetic-field curvature radii (**Figure 5H**) may all contribute to the heating of the observed cold ions from the lobe into the ion jet. However, one should note that the temperature results have a large uncertainty from our partial-moment calculation. As shown in **Figures 3**; **Supplementary Figures S3**, the thermal parts of the hot and cold populations usually overlap with each other. We cut major parts of the cold-ion VDFs empirically by eye. The results of the number density and bulk velocity are relatively reliable, but the ambient treatment of the VDF boundaries brings large errors to the temperature. The temperature results can be improved by fitting the cold-ion VDFs in the three-dimensional velocity space, which will be tried in our future works.

## 4 CONCLUSION

We investigated an MMS magnetotail crossing from 21:30:00 UT to 24:00:00 UT on July 06, 2017 with cold ions and ongoing

magnetic reconnection and present quantitative analysis of the cold ions inside a reconnection ion jet. In this event, MMS cross one tailward and two earthward ion jets, and we explored the three-dimensional ion VDFs and find types of ion VDFs with cold-ion beams. MMS observe hot ions of plasma-sheet origin throughout the tailward jet and the first earthward ion jet, and cold ions with small $\mathbf{V}_B$ show up in part of the jet crossing. At the separatrix, MMS observe $\mathbf{E}\times\mathbf{B}$ drifting cold ions with negligible $\mathbf{V}_B$. The second earthward ion jet is lead by a dipolarization front, and we find four types of ion VDFs inside: Type I consists of only a single hot plasma-sheet population, Type II consists of a hot population and a cold population with a positive $\mathbf{V}_B$, Type III consists of a hot population and a cold population with a negative $\mathbf{V}_B$, and Type IV consists of a hot population with counter-streaming cold populations. Our analysis focuses on those VDFs with cold-ion beams. The occurrence rate of Type II VDFs decreases gradually from the southern to the northern sides of the neutral line. Conversely, the occurrence rate of Type III VDFs increase gradually from south to the north. The occurrence rate of Type IV peaks at the neutral line. This distribution of VDFs could be formed by the patchy cold-ion inflow, the bouncing motions within the divergent Hall electrostatic potential well, and the scattering effect due to plasma waves and the curved magnetic field lines with small curvature radii.

We adopted the same technique as used in Li et al. (2017) to compute the partial moments of the hot and cold populations of Types II, III and IV VDFs. The average number density of the cold-ion beams is approximately 13% of that of the hot ions, meaning that the cold ions are a minor population in this investigated event. All the hot and cold ions are outflow ions towards Earth. The average bulk speed of the cold-ion beams is approximately 38% larger than that of the hot plasma-sheet ions. This extra speed is predominantly along the magnetic field direction. Those cold-ion beams could come from the cold-ion diffusion region and be initially accelerated by the Hall electric field. Then, the accelerated cold-ion beams could be further accelerated by the shrinking field lines through the Fermi effect. The cold-ion beams are still one order of magnitude colder than the hot ions, while the electric field with large gradient at the separatrix and the scattering effect by the waves and highly curved magnetic field lines may thermalize those cold ions from the lobe into the ion jet.

## DATA AVAILABILITY STATEMENT

All data used in this work are available at the MMS Data Center (https://lasp.colorado.edu/mms/sdc/public/). Data analysis was performed using the IRFU-MATLAB package (https://github.com/irfu/irfu-matlab).

## AUTHOR CONTRIBUTIONS

WL, YL, and BT carried out the data analysis and interpretation. YL wrote the first-version article, and WL revised it. CN, JH, CW, and QZ contributed to the data interpretation and article preparation. JB led the design and operation of the MMS mission. The remaining co-authors contributed to the data analysis under the framework of an ISSI international team.

## FUNDING

This work was supported by NNSFC Grant No. 41731070, 41974170, and 41974196, the Chinese Academy of Sciences (QYZDJSSW-JSC028, XDA15052500, XDA17010301 and XDB41000000), and the Specialized Research Fund for State Key Laboratories of China. WYL was also supported by the Youth Innovation Promotion Association (2018177), and the Young Elite Scientists Sponsorship Program by CAST and the Open Research Program of Key Laboratory of Geospace Environment CAS. CN received support from the Research Council of Norway under contract 300865.

## ACKNOWLEDGMENTS

We thank the MMS team and instrument principal investigators for data access and support. We acknowledge support from the International Space Science Institute (ISSI) international team *Cold plasma of ionospheric origin in the Earth's magnetosphere*.

## SUPPLEMENTARY MATERIAL

The Supplementary Material for this article can be found online at: https://www.frontiersin.org/articles/10.3389/fspas.2021.745264/full#supplementary-material

## REFERENCES

Alm, L., André, M., Vaivads, A., Khotyaintsev, Y. V., Torbert, R. B., Burch, J. L., et al. (2018). Magnetotail hall physics in the presence of cold ions. *Geophys. Res. Lett.* 45 (10941–10), 950. doi:10.1029/2018GL079857

André, M., and Cully, C. M. (2012). Low-energy ions: A previously hidden solar system particle population. *Geophys. Res. Lett.* 39, L03101. doi:10.1029/2011GL05024210.1029/2011gl050242

André, M., Li, K., and Eriksson, A. I. (2015). Outflow of low-energy ions and the solar cycle. *J. Geophys. Res. Space Phys.* 120, 1072–1085. doi:10.1002/2014JA02071410.1002/2014ja020714

André, M., Li, W., Toledo-Redondo, S., Khotyaintsev, Y. V., Vaivads, A., Graham, D. B., et al. (2016). Magnetic reconnection and modification of the hall physics due to cold ions at the magnetopause. *Geophys. Res. Lett.* 43, 6705–6712. doi:10.1002/2016GL069665

Angelopoulos, V., Baumjohann, W., Kennel, C. F., Coroniti, F. V., Kivelson, M. G., Pellat, R., et al. (1992). Bursty bulk flows in the inner central plasma sheet. *J. Geophys. Res.* 97, 4027–4039. doi:10.1029/91ja02701

Angelopoulos, V., Kennel, C. F., Coroniti, F. V., Pellat, R., Kivelson, M. G., Walker, R. J., et al. (1994). Statistical characteristics of bursty bulk flow events. *J. Geophys. Res.* 99, 21257–21280. doi:10.1029/94ja01263

Aunai, N., Belmont, G., and Smets, R. (2011). Proton acceleration in antiparallel collisionless magnetic reconnection: Kinetic mechanisms behind the fluid dynamics. *J. Geophys. Res.* 116, a–n. doi:10.1029/2011ja016688

Baumjohann, W., Paschmann, G., and Lühr, H. (1990). Characteristics of high-speed ion flows in the plasma sheet. *J. Geophys. Res.* 95, 3801–3809. doi:10.1029/JA095iA04p03801

Birn, J., Nakamura, R., Panov, E. V., and Hesse, M. (2011). Bursty bulk flows and dipolarization in mhd simulations of magnetotail reconnection. *J. Geophys. Res.* 116, a–n. doi:10.1029/2010ja016083

Birn, J., Runov, A., and Zhou, X. Z. (2017). Ion velocity distributions in dipolarization events: Distributions in the central plasma sheet. *J. Geophys. Res. Space Phys.* 122, 8014–8025. doi:10.1002/2017ja024230

Büchner, J., and Zelenyi, L. M. (1989). Regular and chaotic charged particle motion in magnetotaillike field reversals: 1. basic theory of trapped motion. *J. Geophys. Res.* 94, 11821–11842. doi:10.1029/JA094iA09p11821

Burch, J. L., Moore, T. E., Torbert, R. B., and Giles, B. L. (2016). Magnetospheric Multiscale overview and science objectives. *Space Sci. Rev.* 199, 5–21. doi:10.1007/s11214-015-0164-910.1007/s11214-015-0164-9

Cassak, P. A., and Shay, M. A. (2007). Scaling of asymmetric magnetic reconnection: General theory and collisional simulations. *Phys. Plasmas* 14, 102114. doi:10.1063/1.279563010.1063/1.2795630

Chappell, C. R., Baugher, C. R., and Horwitz, J. L. (1980). New advances in thermal plasma research. *Rev. Geophys.* 18, 853–861. doi:10.1029/RG018i004p00853

Cully, C. M., Donovan, E. F., Yau, A. W., and Arkos, G. G. (2003). Akebono/Suprathermal mass spectrometer observations of low-energy ion outflow: Dependence on magnetic activity and solar wind conditions. *J. Geophys. Res.* 108, 1093. doi:10.1029/2001JA009200

Dai, L., Wang, C., and Lavraud, B. (2021). Kinetic imprints of ion acceleration in collisionless magnetic reconnection. *ApJ* 919, 15. doi:10.3847/1538-4357/ac0fde10.3847/1538-4357/ac0fde

Dargent, J., Aunai, N., Lavraud, B., Toledo-Redondo, S., and Califano, F. (2019). Signatures of cold ions in a kinetic simulation of the reconnecting magnetopause. *J. Geophys. Res. Space Phys.* 124, 2497–2514. doi:10.1029/2018JA026343

Dargent, J., Aunai, N., Lavraud, B., Toledo-Redondo, S., and Califano, F. (2020). Simulation of plasmaspheric plume impact on dayside magnetic reconnection. *Geophys. Res. Lett.* 47, e2019GL086546. doi:10.1029/2019gl086546

Dargent, J., Aunai, N., Lavraud, B., Toledo-Redondo, S., Shay, M. A., Cassak, P. A., et al. (2017). Kinetic simulation of asymmetric magnetic reconnection with cold ions. *J. Geophys. Res. Space Phys.* 122, 5290–5306. doi:10.1002/2016JA023831

Divin, A., Khotyaintsev, Y. V., Vaivads, A., André, M., Toledo-Redondo, S., Markidis, S., et al. (2016). Three-scale structure of diffusion region in the presence of cold ions. *J. Geophys. Res. Space Phys.* 121, 12001–12013. doi:10.1002/2016JA02360610.1002/2016ja023606

Eastwood, J. P., Goldman, M. V., Hietala, H., Newman, D. L., Mistry, R., and Lapenta, G. (2015). Ion reflection and acceleration near magnetotail dipolarization fronts associated with magnetic reconnection. *J. Geophys. Res. Space Phys.* 120, 511–525. doi:10.1002/2014ja020516

Eastwood, J. P., Phan, T.-D., Mozer, F. S., Shay, M. A., Fujimoto, M., Retinò, A., et al. (2007). Multi-point observations of the hall electromagnetic field and secondary island formation during magnetic reconnection. *J. Geophys. Res.* 112, a–n. doi:10.1029/2006ja012158

Engwall, E., Eriksson, A. I., Cully, C. M., André, M., Torbert, R., and Vaith, H. (2009). Earth's ionospheric outflow dominated by hidden cold plasma. *Nat. Geosci* 2, 24–27. doi:10.1038/ngeo387

Ergun, R. E., Tucker, S., Westfall, J., Goodrich, K. A., Malaspina, D. M., Summers, D., et al. (2016). The axial double probe and fields signal processing for the MMS mission. *Space Sci. Rev.* 199, 167–188. doi:10.1007/s11214-014-0115-x

Fu, H. S., Cao, J. B., Khotyaintsev, Y. V., Sitnov, M. I., Runov, A., Fu, S. Y., et al. (2013). Dipolarization fronts as a consequence of transient reconnection: *In situ* evidence. *Geophys. Res. Lett.* 40, 6023–6027. doi:10.1002/2013GL058620

Fujimoto, M., Nakamura, M. S., Nagai, T., Mukai, T., Yamamoto, T., and Kokubun, S. (1996). New kinetic evidence for the near-earth reconnection. *Geophys. Res. Lett.* 23, 2533–2536. doi:10.1029/96GL02429

Gershman, D. J., Dorelli, J. C., Avanov, L. A., Gliese, U., Barrie, A., Schiff, C., et al. (2019). Systematic Uncertainties in Plasma Parameters Reported by the Fast Plasma Investigation on NASA's Magnetospheric Multiscale Mission. *J. Geophys. Res. Space Phys.* 124, 10345–10359. doi:10.1029/2019JA026980

Graham, D. B., Khotyaintsev, Y. V., Norgren, C., Vaivads, A., André, M., Toledo-Redondo, S., et al. (2017). Lower hybrid waves in the ion diffusion and magnetospheric inflow regions. *J. Geophys. Res. Space Phys.* 122, 517–533. doi:10.1002/2016JA02357210.1002/2016ja023572

Hietala, H., Drake, J. F., Phan, T. D., Eastwood, J. P., and McFadden, J. P. (2015). Ion temperature anisotropy across a magnetotail reconnection jet. *Geophys. Res. Lett.* 42, 7239–7247. doi:10.1002/2015gl065168

Hoshino, M., Mukai, T., Yamamoto, T., and Kokubun, S. (1998). Ion dynamics in magnetic reconnection: Comparison between numerical simulation and geotail observations. *J. Geophys. Res.* 103, 4509–4530. doi:10.1029/97ja01785

Kistler, L. M., and Mouikis, C. G. (2016). The inner magnetosphere ion composition and local time distribution over a solar cycle. *J. Geophys. Res. Space Phys.* 121, 2009–2032. doi:10.1002/2015JA021883

Li, K., Haaland, S., Eriksson, A., André, M., Engwall, E., Wei, Y., et al. (2013). Transport of cold ions from the polar ionosphere to the plasma sheet. *J. Geophys. Res. Space Phys.* 118, 5467–5477. doi:10.1002/jgra.50518

Li, W. Y., André, M., Khotyaintsev, Y. V., Vaivads, A., Fuselier, S. A., Graham, D. B., et al. (2017). Cold ionospheric ions in the magnetic reconnection outflow region. *J. Geophys. Res. Space Phys.* 122 (10), 10194–10202. doi:10.1002/2017ja024287

Lindqvist, P.-A., Olsson, G., Torbert, R. B., King, B., Granoff, M., Rau, D., et al. (2016). The spin-plane double probe electric field instrument for MMS. *Space Sci. Rev.* 199, 137–165. doi:10.1007/s11214-014-0116-9

Moore, T. E., Chappell, C. R., Chandler, M. O., Craven, P. D., Giles, B. L., Pollock, C. J., et al. (1997). High-altitude observations of the polar wind. *Science* 277, 349–351. doi:10.1126/science.277.5324.349

Nagai, T., Fujimoto, M., Saito, Y., Machida, S., Terasawa, T., Nakamura, R., et al. (1998). Structure and dynamics of magnetic reconnection for substorm onsets with geotail observations. *J. Geophys. Res.* 103, 4419–4440. doi:10.1029/97ja0219010.1029/97ja02190

Nakamura, R., Baumjohann, W., Klecker, B., Bogdanova, Y., Balogh, A., Rème, H., et al. (2002). Motion of the dipolarization front during a flow burst event observed by cluster. *Geophys. Res. Lett.* 29, 3–1. –3–4. doi:10.1029/2002GL015763

Norgren, C., Tenfjord, P., Hesse, M., Toledo-Redondo, S., Li, W.-Y., Xu, Y., et al. (2021). On the presence and thermalization of cold ions in the exhaust of antiparallel symmetric reconnection. *Front. Astron. Space Sci.* 8, 149. doi:10.3389/fspas.2021.730061

Pollock, C., Moore, T., Jacques, A., Burch, J., Gliese, U., Saito, Y., et al. (2016). Fast Plasma Investigation for Magnetospheric Multiscale. *Space Sci. Rev.* 199, 331–406. doi:10.1007/s11214-016-0245-4

Priest, E., and Forbes, T. (2007). *Magnetic reconnection.* Magnetic Reconnection. Cambridge, UK: Cambridge University Press.

Runov, A., Angelopoulos, V., Artemyev, A., Birn, J., Pritchett, P. L., and Zhou, X. Z. (2017). Characteristics of ion distribution functions in dipolarizing flux bundles: Event studies. *J. Geophys. Res. Space Phys.* 122, 5965–5978. doi:10.1002/2017ja02401010.1002/2017ja024010

Runov, A., Angelopoulos, V., Sitnov, M. I., Sergeev, V. A., Bonnell, J., McFadden, J. P., et al. (2009). Themis observations of an earthward-propagating dipolarization front. *Geophys. Res. Lett.* 36. doi:10.1029/2009GL038980

Russell, C. T., Anderson, B. J., Baumjohann, W., Bromund, K. R., Dearborn, D., Fischer, D., et al. (2016). The Magnetospheric Multiscale Magnetometers. *Space Sci. Rev.* 199, 189–256. doi:10.1007/s11214-014-0057-310.1007/978-94-024-0861-4_8

Sauvaud, J.-A., Louarn, P., Fruit, G., Stenuit, H., Vallat, C., Dandouras, J., et al. (2004). Case studies of the dynamics of ionospheric ions in the Earth's magnetotail. *J. Geophys. Res.* 109. doi:10.1029/2003JA009996

Shay, M. A., Drake, J. F., Denton, R. E., and Biskamp, D. (1998). Structure of the dissipation region during collisionless magnetic reconnection. *J. Geophys. Res.* 103, 9165–9176. doi:10.1029/97ja03528

Tenfjord, P., Hesse, M., Norgren, C., Spinnangr, S. F., and Kolstø, H. (2019). The impact of oxygen on the reconnection rate. *Geophys. Res. Lett.* 46, 6195–6203. doi:10.1029/2019gl082175

Toledo-Redondo, S., André, M., Vaivads, A., Khotyaintsev, Y. V., Lavraud, B., Graham, D. B., et al. (2016b). Cold ion heating at the dayside magnetopause during magnetic reconnection. *Geophys. Res. Lett.* 43, 58–66. doi:10.1002/2015GL067187

Toledo-Redondo, S., André, M., Aunai, N., Chappell, C. R., Dargent, J., Fuselier, S. A., et al. (2021). Impacts of ionospheric ions on magnetic reconnection and earth's magnetosphere dynamics. *Rev. Geophys. n/a*, e2020RG000707. doi:10.1029/2020RG000707

Toledo-Redondo, S., André, M., Khotyaintsev, Y. V., Vaivads, A., Walsh, A., Li, W., et al. (2016a). Cold ion demagnetization near the x-line of magnetic reconnection. *Geophys. Res. Lett.* 43, 6759–6767. doi:10.1002/2016GL069877

Toledo-Redondo, S., Dargent, J., Aunai, N., Lavraud, B., André, M., Li, W., et al. (2018). Perpendicular current reduction caused by cold ions of ionospheric origin in magnetic reconnection at the magnetopause: Particle-in-cell simulations and spacecraft observations. *Geophys. Res. Lett.* 45, 10,033–10,042. doi:10.1029/2018GL079051

Toledo-Redondo, S., Vaivads, A., André, M., and Khotyaintsev, Y. V. (2015). Modification of the Hall physics in magnetic reconnection due to cold ions at the Earth's magnetopause. *Geophys. Res. Lett.* 42, 6146–6154. doi:10.1002/2015GL06512910.1002/2015gl065129

Walsh, B. M., Phan, T. D., Sibeck, D. G., and Souza, V. M. (2014). The plasmaspheric plume and magnetopause reconnection. *Geophys. Res. Lett.* 41, 223–228. doi:10.1002/2013GL058802

Wang, S., Kistler, L. M., Mouikis, C. G., Liu, Y., and Genestreti, K. J. (2014). Hot magnetospheric O + and cold ion behavior in magnetopause reconnection: Cluster observations. *J. Geophys. Res. Space Phys.* 119, 9601–9623. doi:10.1002/2014JA02040210.1002/2014ja020402

Welling, D. T., André, M., Dandouras, I., Delcourt, D., Fazakerley, A., Fontaine, D., et al. (2015). The earth: Plasma sources, losses, and transport processes. *Space Sci. Rev.* 192, 145–208. doi:10.1007/s11214-015-0187-2

Wygant, J. R., Cattell, C. A., Lysak, R., Song, Y., Dombeck, J., McFadden, J., et al. (2005). Cluster observations of an intense normal component of the electric field at a thin reconnecting current sheet in the tail and its role in the shock-like acceleration of the ion fluid into the separatrix region. *J. Geophys. Res.* 110. doi:10.1029/2004ja010708

Xu, Y., Fu, H. S., Norgren, C., Toledo-Redondo, S., Liu, C. M., and Dong, X. C. (2019). Ionospheric cold ions detected by mms behind dipolarization fronts. *Geophys. Res. Lett.* 46, 7883–7892. doi:10.1029/2019gl083885

Yamada, M., Kulsrud, R., and Ji, H. (2010). Magnetic reconnection. *Rev. Mod. Phys.* 82, 603–664. doi:10.1103/RevModPhys.82.603

Yamauchi, M. (2019). Terrestrial ion escape and relevant circulation in space. *Ann. Geophys.* 37, 1197–1222. doi:10.5194/angeo-37-1197-2019

Young, D. T., Burch, J. L., Gomez, R. G., De Los Santos, A., Miller, G. P., Wilson, P., et al. (2016). Hot plasma composition analyzer for the magnetospheric multiscale mission. *Space Sci. Rev.* 199, 407–470. doi:10.1007/s11214-014-0119-6

Zaitsev, I., Divin, A., Semenov, V., Kubyshkin, I., Korovinskiy, D., Deca, J., et al. (2021). Cold ion energization at separatrices during magnetic reconnection. *Phys. Plasmas* 28, 032104. doi:10.1063/5.0008118

**Conflict of Interest:** The authors declare that the research was conducted in the absence of any commercial or financial relationships that could be construed as a potential conflict of interest.

**Publisher's Note:** All claims expressed in this article are solely those of the authors and do not necessarily represent those of their affiliated organizations, or those of the publisher, the editors, and the reviewers. Any product that may be evaluated in this article, or claim that may be made by its manufacturer, is not guaranteed or endorsed by the publisher.